ICAS 2016
30th Congress of the International Council of the Aeronautical Sciences
DCC, Daejeon, Korea ; September 25-30, 2016

LOW-DRAG / LOW-BOOM SHAPE OPTIMIZATION OF A BIPLANE WING / TWIN-BODY FUSELAGE SST CONFIGURATION

Naohiko BAN*
Department of Energy & Environmental Engineering, Nagaoka University of Technology

Keywords: *CFD, Supersonic Transport, Multi-disciplinary Optimization, Sonic Boom*

Abstract

The generation of shock waves is inevitable in supersonic cruise which results in the generation of wave drag as well as sonic boom on the ground. Some innovative concepts as supersonic biplane concept and supersonic twin-body fuselage concept have been proposed in recent to reduce the supersonic wave drag dramatically. In this study, the aerodynamic and sonic boom performance of innovative supersonic transport (SST) wing-body configurations is discussed by numerical approaches. This study is performed to obtain design knowledge for the innovative SST by using an optimization method of Kriging response surface model and genetic algorithm. The wing section shape and body shape of the biplane / twin-body model is optimized under the conditions of design Mach number of 1.7 and angle of attack of 2 degrees. The optimized results show the tradeoff relationship between lift-drag ratio and maximum overpressure of sonic boom distribution on the ground. The optimization results revealed the important points to improve the aerodynamic and sonic boom performances of the innovative SST configuration.

1 Introduction

Supersonic transport “Concorde” has an advantage in its cruising speed which overwhelms other conventional transports. However, Concorde has ended its operations in 2003 mainly due to its problems of economical efficiency and environmental burden. Recently, there are many attempts for the realization of next generation supersonic transport. One of them is to reduce strong shock waves by the interference of them. The reduction of shock waves will contribute to reduce wave drag and sonic boom that are beneficial for low-boom / low-drag SST. In this research, supersonic biplane concept and supersonic twin-body concept are adopted to reduce supersonic wave drag.

In the supersonic biplane concept, the strength of wave drag has been successfully reduced by the interference of shock waves between the biplanes[1-4]. According to Ref.[1], the wave drag at zero lift of the biplane airfoil was reduced by nearly 90% compared to an equal volume diamond-wedge airfoil in two dimensional inviscid simulations.

A twin-body fuselage concept[5] has also been proposed to reduce the wave drag due to the fuselage volume of aircraft. According to Ref.[5], over 20% total drag reduction was achieved by an optimized twin-body fuselage compared with the Sears-Haack (S.H.) single-body fuselage under the constraint of fixed fuselage volume. This has been achieved by reducing the interference drag between bodies. The S.H. body is well-known as the supersonic single-body configuration which has the lowest wave drag for specified volume and length[6].

The fusion of the two advanced concepts yields an innovative SST configuration which is a biplane wing / twin-body fuselage configuration. It was proved that the innovative wing-body SST configuration was aerodynamically effective for the reduction of wave drag with a large-sized twin-body (about for 400 passengers)[7]. However, the lift-drag ratio (L/D) of the 400 passengers model is less than 5 while that of Concorde is known to be as

about 7~8 (at freestream Mach number M_∞ of 2.0). The one of the major reasons is its larger fuselage volume than Concorde[8]. In this study, therefore, the biplane wing / twin-body fuselage configuration (Fig. 1) is designed with its half-sized body, and its aerodynamic / sonic boom performance is investigated.

In this research, three design optimization problems are solved to obtain design knowledge of the innovative SST configuration. The shape optimizations are performed to achieve successful shock interactions and to improve the aerodynamic / sonic boom performance.

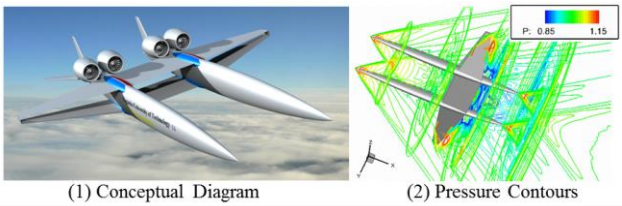

(1) Conceptual Diagram (2) Pressure Contours

Fig. 1 Twin-Body Fuselage / Biplane Wing Configuration

2 Computational Methodologies

2.1 CFD Approaches

Three-dimensional supersonic inviscid flows are analyzed by an unstructured mesh CFD solver of TAS (Tohoku University Aerodynamic Simulation)-code[9-10]. Compressible Euler equations are solved by a finite-volume cell-vertex scheme. The numerical flux normal to the control volume boundary is computed using the approximate Riemann solver of Harten-Lax-van Leer-Einfelds-Wada (HLLEW)[11]. The second-order spatial accuracy is achieved by the Unstructured MUSCL (U-MUSCL) approach [10,12] with Venkatakrishnan's limiter[13]. The Lower-Upper Symmetric Gauss-Seidel (LU-SGS) implicit method for unstructured meshes[14] is used for the time integration. Three-dimensional unstructured meshes are generated using the TAS-mesh package, which includes surface mesh generation by an advancing front approach[15] and tetrahedral volume mesh generation by a Delaunay approach[16]. The high accuracy of this unstructured mesh CFD approach has already been confirmed in literature[10].

2.2 Sonic Boom Analysis

The sonic booms on the ground are predicted by a nonlinear acoustic propagation solver of Xnoise[17-18] which has been developed by Japan Aerospace Exploration Agency (JAXA). An augmented Burgers equation is numerically solved by using the operator splitting method, which takes into account the effects of nonlinearity, geometrical spreading, inhomogeneity of atmosphere, thermo-viscous attenuation and molecular vibration relaxation. In this approach, initial (input) pressure distributions are extracted from CFD solutions on the lower side of SST configurations. Then the propagation of the pressure distribution to the ground is solved by the augmented Burgers equation. We investigated the influence of the extracted position of the initial pressure distribution, which indicated that the extraction at two fuselage lengths below was sufficient for accurate sonic boom evaluation in this study.

2.3 Skin Friction Drag Estimation

In this research, skin friction drags of various SST configurations are estimated by introducing simple algebraic skin friction models. Assuming that the boundary layer along the body is fully turbulent, the skin friction drag coefficient can be estimated as:

$$C_{Df} = C_f \frac{S_{wet}}{S_{ref}} \qquad (1)$$

where C_f is the averaged turbulent skin friction coefficient on the wetted area of the body, and S_{wet} and S_{ref} are respectively the wetted area of the body and reference area. The skin friction coefficient for turbulent boundary layer conditions can be calculated by the following Prandtl-Schlichting flat-plate skin friction formula[19-21]:

$$C_f = \frac{0.455}{(\log_{10}\mathrm{Re})^{2.58}\left(1+0.144M_\infty^2\right)^{0.65}} \qquad (2)$$

where Re and M_∞ are respectively the Reynolds number and freestream Mach number. In this research, the Reynolds number is given from the cruise condition of Concorde (total length of 62[m]). Since the speed of sound (a_∞) and kinematic viscosity (ν_∞) at the altitude of

18,000[m] are respectively 295.069[m/s] and 1.1686×10^{-4}[m^2/s] according to Ref.[21], the Reynolds number for the fuselage body is calculated as:

$$\mathrm{Re} = \frac{M_\infty a_\infty l}{\nu_\infty} \cong 266\times10^6 \qquad (3)$$

The Reynolds number for the main wing is calculated in the same manner with its mean chord length (*Re*:32.5×10^6, mean chord length:0.122*l*). The skin friction drag coefficients of the fuselage and wing are separately estimated with the corresponding Reynolds numbers by using Eqs.(1-2). In Refs.[1,2,22], predicted friction drags based on the algebraic skin friction models are compared with those based on viscous CFD computations. It has been concluded that the simple algebraic skin friction models are reasonably accurate for the prediction of friction drag in supersonic flows.

3 Basic Shape Definition

The section airfoil thickness ratios of the Busemann biplane are set to 5% of the chord length in both the upper and lower wings. Unswept tapered biplane wing configurations are designed in this research for three-dimensional biplane wing. The aspect and taper ratios are respectively set to about 7 and 0.25. The chord length of the main wing at the root section is about *l*/6. A vertical wingtip plate is arranged between the wings to increase the two-dimensionality of the flow around the biplane wing (Fig. 2(2)). The inner side of the wingtip plate is a flat plate shape and its outer side has a thickness distribution based on the S.H. body radius distribution (maximum thickness ratio of 3.36%). For appropriate shock interactions, the vertical distance between the wings is shortened at the outer wing by adding a dihedral angle to the lower wing. The non-dimensional section airfoil shape is same at all span-wise positions.

The cross sectional area distribution of the twin-body configuration is set to that of S.H. body. The volume of the twin-body is set to half of the previous 400 passengers model[8]. The cross sectional shapes of the twin bodies are deformed from circle (conventional S.H. body) to ellipse to reduce wing-body parasite drag (Fig. 2(3)). In this case, the maximum width of a body is about 2.9[m]. Finally, the twin-body / biplane wing configuration can be defined as Fig. 2(4).

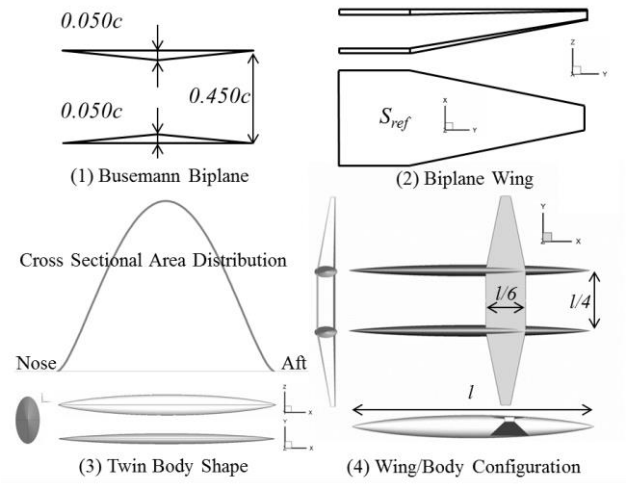

Fig. 2 Basic Shape Definition

4 Shape Optimization

4.1 Computational Condition

The aerodynamic performance is discussed at design freestream Mach number of 1.7 and angle of attack of 2 degrees by using inviscid CFD computations. The increment of skin friction drag has also been discussed utilizing the standard algebraic (turbulent) skin friction models based on the wetted areas of SST configurations. In the sonic boom propagation analyses, standard atmosphere temperature / humidity profiles are utilized. The fuselage length and the cruise altitude are respectively set to 62[m] and 18,000[m], that are given from the conditions of Concorde.

4.2 Optimization Method

In this study, a surrogate model-based global design optimization method is utilized which makes use of a Kriging response surface model. An ordinary Kriging surrogate model[23-24] is used to construct the surrogate models of aerodynamic functions in design variables space. Firstly, initial sample points are generated in the design variables space by a

Latin Hypercube Sampling (LHS) method, and then these are evaluated by CFD computations. By using the information of the initial sample points, initial surrogate models are constructed. The search of a promising location in the design variables space is executed by a real-coded multi-objective genetic algorithm[25] on the surrogate models. The promising locations are explored by the criteria of expected improvement (EI)[24]. The function of EI expresses a potential for improvement in design variables space which considers both estimated function value as well as uncertainty of the surrogate model. The CFD computations are executed for the explored promising locations where EI is maximal, and then new surrogate models are created by adding its information. By the iterative process described above, the accuracies of the surrogate models are efficiently increased around the promising locations in the design variables space.

4.3 Design Variables Definition

In this study, three multi-disciplinary design optimizations are performed to obtain design knowledge for the twin-body / biplane-wing configuration. The first is the wing section shape optimization with three design variables as its fundamental wing shape design. The second is the wing section shape optimization with twelve design variables as its detailed wing shape design. The third is the wing-body shape optimization with twenty-four design variables. The initial geometry of all optimizations is the model defined in section 3. The deformed sectional shape of biplane is employed at all span positions. The body near the wing is deformed by using an unstructured dynamic mesh method based on spring analogy[26].

4.3.1 Basic Wing Section Shape Optimization

Three design variables are utilized to modify x and z coordinates of the mid-chord apexes of the upper and lower wings (Fig. 3(1)), since it is assumed that the inner side shapes of biplane are important to achieve successful shock interactions. This definition enables a constant wing volume automatically during the optimization process.

4.3.2 Detailed Wing Section Shape Optimization

The biplane airfoil is expressed by Bezier curves (Fig. 3(2)). In addition to the deformation of the mid-chord apexes (dv4, dv5, dv6 and dv7), other five design variables (dv2, dv3, dv8, dv9 and dv12) are set to deform the inner side shapes of biplane. The shapes of the lower-surface of the lower-wing are considered to be important for the pressure waves propagating to the ground, which means important to improve the sonic boom performance. Therefore, two design variables (dv10 and dv11) are added to deform the biplane shapes. On the other hand, the shapes of the upper-surface of the upper-wing are considered to be not important for the pressure waves propagating to the ground. Therefore, only one design variable (dv1) is added to control the total section area of the wing.

4.3.3 Wing-Body Shape Optimization

Supersonic area rule has also been introduced to reduce the wave drag due to the interactions between wing-body by smoothing the equivalent cross-sectional area distribution considering planes inclined at the Mach angle[27]. Thus, it is assumed that the definition of the body shapes is important to reduce the parasite drag. In this research, the body cross-sectional area distribution is defined as the following expression.

$$S(\theta)=\frac{l^2}{4}\left\{A_1\left(\pi-\theta+\frac{\sin 2\theta}{2}\right)+\sum_{n=2}^{\infty}A_n\left(\frac{\sin(n+1)\theta}{n+1}-\frac{\sin(n-1)\theta}{n-1}\right)\right\} \quad (4)$$

where l and A_n are respectively the fuselage length and coefficients. θ is the parameter which expresses the coordinate x defined as:

$$x=\frac{l}{2}(1+\cos\theta),\quad (\pi\geq\theta\geq 0) \quad (5)$$

The object expressed only with the term of A_1 is known as the von Karman ogive body which has a sharp angled shape at the one side. The object expressed only with the term of A_2 is known as the Sears-Haack body which has sharp angled shapes at the both side. The object with the terms of A_3 and more is able to express complicated shapes. In this study, the body shape is expressed with the terms of A_2~A_7 and these coefficients are defined as design variables. The inner / outer side shapes of the

body are separately defined by the six design variables. In addition to these twelve design variables for the twin bodies, other 12 design variables of Fig. 3(2) are utilized to define the biplane wing shape.

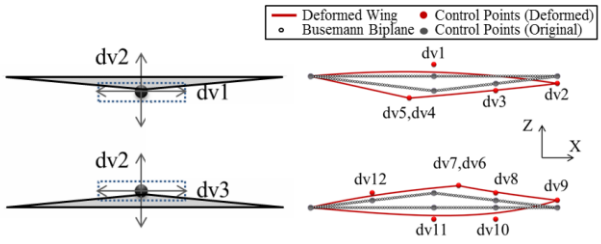

(1) Wing Shape Modification of First Optimization

(2) Wing Shape Modification of Second and Third Optimizations

Fig. 3 Wing Shape Parameterizations

4.4 Objective Functions & Constraints

4.4.1 Basic Wing Section Shape Optimization

The maximization of *L/D* and the minimization of maximum overpressure (P_{max}) which is the peak pressure value of a propagated pressure distribution on ground are the objective functions of this problem. The wing volume is kept constant automatically in this problem as explained in 4.3.1.

4.4.2 Detailed Wing Section Shape Optimization

The objective functions are the same as 4.4.1. Two constraints are given in this optimization. A constraint is given on the total sectional area of new designed wing (S_{total}), which should be larger than that of the original Busemann biplane wing. The other is given on the sectional area of new designed upper wing (S_{upper}), which should be larger than the half of the original Busemann biplane wing. These are specified because very thin airfoils are not realistic structurally.

4.4.3 Wing-Body Shape Optimization

The maximization of *L/D* and the minimization of A-weighted sound exposure level (L_{AE})[28] which is a metric to express subjective loudness of sonic boom are the objective functions of this problem. Both of P_{max} and L_{AE} are metrics to evaluate the sonic boom intensity. In addition to the two constraints of 4.4.2, other two constraints are given in this optimization. A constraint is given on the total volume of new designed body (V_{body}), which should be larger than that of the original Sears-Haack body to preserve the space for 200 passengers. The other is given on the minimum ellipticity of new designed body (E_{min}), which should be larger than the half of the original Sears-Haack body in the range of $x/l>0.5$. This is also because very thin bodies are not realistic structurally. The objective functions and constraints of the three optimization problems are summarized in Table 1.

Table 1 Objective Functions and Constraints

	Objective Function			Constraint				
	L/D	P_{max}	L_{AE}	S_{upper}	S_{total}	V_{body}	E_{min}	*dvs*
First Optimization	○	○						3
Second Optimization	○	○		○	○			12
Third Optimization	○		○	○	○	○	○	24

4.5 Results and Discussion

Fig. 4 shows the performances of obtained solutions of the multi-objective low-boom / low-drag shape optimizations. The tradeoff relationship between *L/D* and P_{max} can be observed. The aerodynamic / sonic boom performance of representative models is summarized in Table 2. It is confirmed that better Pareto optimal solutions are obtained with larger numbers of design variables. It is also confirmed that the aerodynamic performance is mainly affected by the wing shape, and the body shape only affects the sonic boom performance. The schematic sketches of obtained design knowledge are summarized in Fig. 5. Those details are discussed in the following sections.

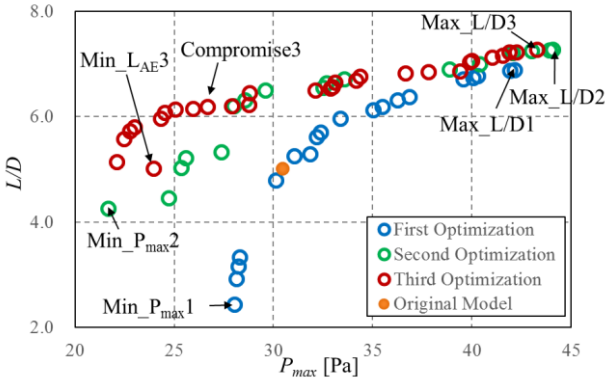

Fig. 4 Comparison of Optimization Results

Table 2 Aerodynamic / Sonic Boom Performance of Representative SST Configurations at M_∞=1.7 and angle of attack of 2 degrees

	C_L	C_{DP}	C_{Df}	L/D	P_{max}	L_{AE}
Busemann	0.120	0.0120	0.0120	5.02	30.5	78.8
Min_P_{max}1	0.065	0.0148	0.0120	2.43	28.1	79.3
Min_P_{max}2	0.102	0.0119	0.0120	4.25	21.7	77.4
Min_L_{AE}3	0.132	0.0149	0.0123	4.85	24.1	75.8
Max_L/D1	0.212	0.0187	0.0120	6.89	42.4	82.5
Max_L/D2	0.233	0.0201	0.0120	7.27	44.1	82.8
Max_L/D3	0.233	0.0198	0.0121	7.32	43.8	82.7
Compromise3	0.176	0.0160	0.0122	6.23	27.3	78.0

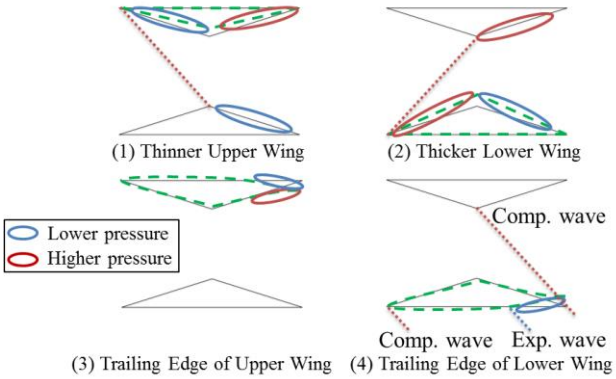

Fig. 5 Schematic Sketches of Effects of Representative Wing Deformations

4.5.1 Basic Wing Section Shape Optimization

In this problem, two optimal designs are selected for comparison, that are named as Max_L/D1 and Min_P_{max}1. The Max_L/D1 has the highest value of L/D while the Min_P_{max}1 has the lowest value of P_{max}. It can be observed that the Max_L/D1 has thicker lower-wing than the upper-wing (Fig. 6(1)). The thicker lower-wing leads to strong shock wave at the leading edge of the lower-wing. The strong shock wave impacts to the upper-wing and leads to higher C_L at the rear/lower-side of the upper-wing (Fig. 5(2)). The thinner upper-wing leads to weak shock wave at the leading edge of the upper-wing. The weak shock wave impacts to the lower wing and leads to higher C_L at the rear/upper-side of the lower-wing (Fig. 5(1)). It is also confirmed from Fig. 6(2) that the Max_L/D1 has the higher C_L at $0.5<x/c<0.9$ in the upper-wing. On the other hand, the strong shock wave is reflected at the rear/lower-side of the upper-wing and propagates toward the ground (Fig. 6(3)). Then, the reflected shock wave is merged with shock waves generated from the nose of body in the propagation process. As a result, Max_L/D1 has larger P_{max} as shown in Fig. 6(4).

Since we have used only three design variables in this optimization, the distributions of objective functions can be visualized in the three-dimensional design variables space. The response surfaces of L/D and P_{max} are visualized in Fig. 7. The x, y and z coordinates are normalized by the ranges of the design variables. It can be observed that L/D is increased with larger dv2 while lower P_{max} is realized with lower dv2. Thus, it is confirmed that dv2 (the thickness difference between upper/lower-wings) has a significant influence on the tradeoff relationship between L/D and P_{max}.

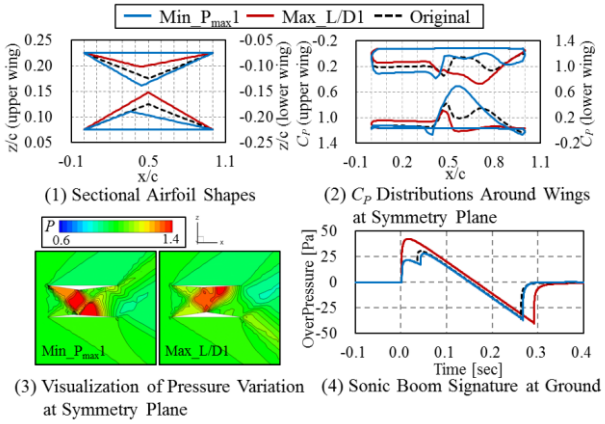

Fig. 6 Results of Basic Wing Section Shape Optimization

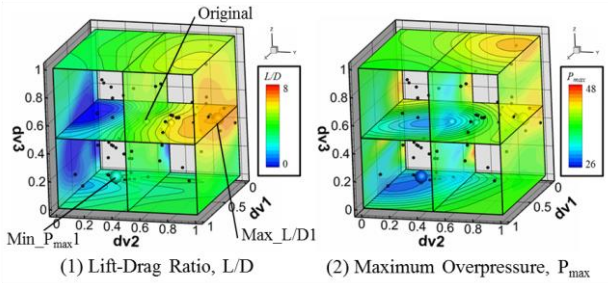

Fig. 7 Visualizations of Response Surfaces of Objective Functions

4.5.2 Detailed Wing Section Shape Optimization

In this problem, two optimal designs are selected for comparison, that are named as Max_L/D2 and Min_P_{max}2. It is confirmed from Fig. 8(1) that Max_L/D2 has thicker lower-wing than the upper-wing as the design knowledge

obtained in 4.5.1. In addition, the Max_L/D2 has a deformation in the downward direction at the trailing edge of the upper-wing (Fig. 5(3)). This deformation leads to lower pressure at the rear/upper-side of the upper-wing ($0.6<x/c<1.0$) and higher pressure at the rear/lower-side of the upper-wing ($0.85<x/c<1.0$) as shown in Fig. 8(2). The lower pressure at the upper-side leads to increase in C_L and the higher pressure at the rear/lower-side leads to increase in C_L and decrease in C_{DP}. Thus, the deformation in the downward direction at the trailing edge of the upper-wing has a significant influence on L/D.

The Min_P_{max}2 has a deformation in the upward direction at the trailing edge of the lower-wing. This deformation leads to generate a successful waveform pattern of "expansion-compression" under the wings (Fig. 5(4) and Fig. 8(3)). The expansion is generated from the rear-side of the lower-wing. The compression is the reflected wave from the rear/lower-side of the upper-wing. Such shock waves pattern leads to suppress the merging of the shock waves (Fig. 8(4), $45m<X<50m$) in the propagation process. As a result, it is confirmed that the waveform on the ground has two peaks (Fig. 8(5)) while the Max_L/D2 has a typical N wave distribution.

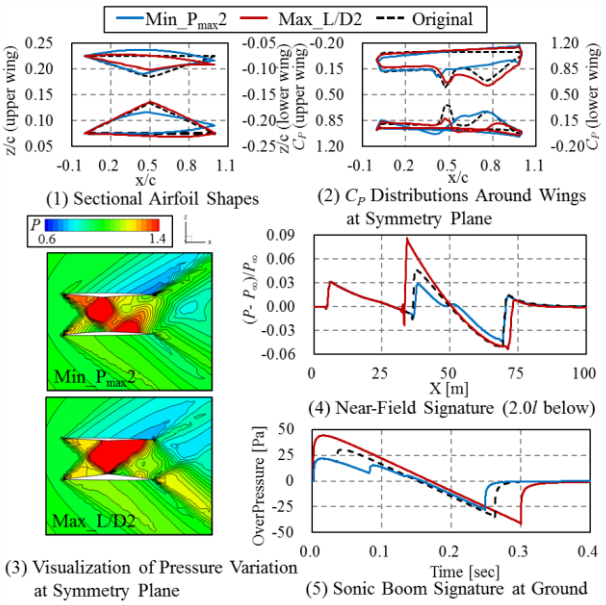

Fig. 8 Results of Detailed Wing Section Shape Optimization

4.5.3 Wing-Body Shape Optimization

In this problem, three optimal designs are selected for comparison, that are named as Max_L/D3, Min_L_{AE}3 and Compromise3. The Compromise3 is a compromised solution selected from the Pareto optimal designs. It is confirmed from Fig. 9 that the higher L/D solutions have larger thickness difference between the upper/lower-wings and the deformation in the downward direction at the trailing edge of the upper-wing. These tendencies are similar with the obtained design knowledge of 4.5.1 and 4.5.2. In addition, it is confirmed from Fig. 10 that the selected optimal models have a same kind of shape deformation of inner body ($x/l \simeq 0.25$). This deformation leads to the reduction of the body-body parasite drag by successful interactions of shock waves. Fig. 11 is the equivalent cross-sectional area distributions of the Max_L/D3 and original model. It is confirmed that the Max_L/D3 has a smoother area distribution than the original model. Thus, it is considered that the Max_L/D3 model introduces the supersonic area rule through this optimization which can contribute to the reduction of the wing-body parasite drag.

It is confirmed from Fig. 9(1) that Min_L_{AE}3 has the deformation in the upward direction at the trailing edge of the lower-wing. This deformation is also the obtained design knowledge of 4.5.2. In addition, it is confirmed from Fig. 10(1) that the Min_L_{AE}3 has a characteristic deformation at the nose of body. The deformation into a blunt body leads to generate strong shock waves at the nose of body. Since stronger shock waves propagate forward faster, the merging of the shock waves can be suppressed by the forward arrangement of strong shock waves (Fig. 12(1)). As a result, it is confirmed that the waveform on the ground has four peaks that are originated from the nose of body, reflected from the body ($x/l \simeq 0.3$), generated from the lower-wing and reflected from the upper-wing (Fig. 13(1)).

It is confirmed from Fig. 9 and Fig. 10 that the Compromise3 has the characteristic deformations about the thickness difference of the wings, the trailing edge shapes of the wings, the nose of body shape and the inner body shapes. This means, in other words, that all

obtained design knowledge appears in the Compromise3. Thus, the obtained Pareto optimal solutions are considered to be designed by assembling the obtained design knowledge. In Fig. 14, the pressure visualizations around the Compromise3 are shown at the flow condition of M_∞ of 1.7 and angle of attack of 2 degrees. We can observe the strong shock waves at the nose of body, the successful interactions of shock waves, and the waveform pattern of "expansion-compression" under the wings.

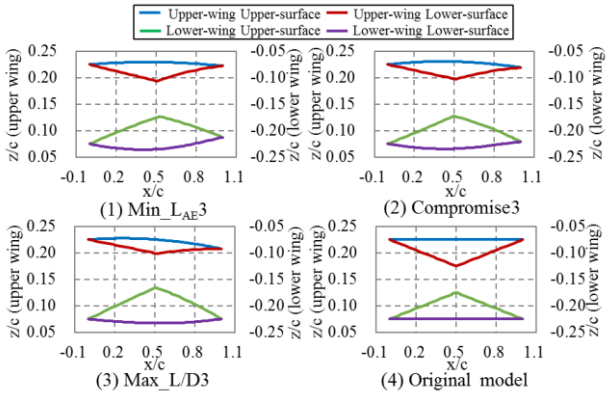

Fig. 9 Sectional Airfoil Shapes

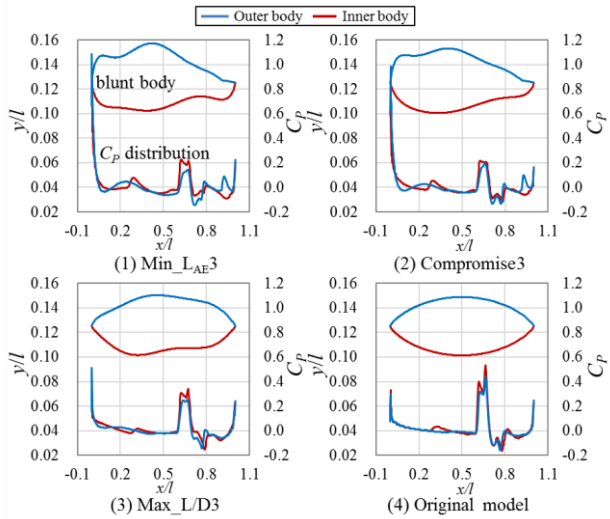

Fig. 10 Sectional Body Shapes and C_P distribution at z=0 plane

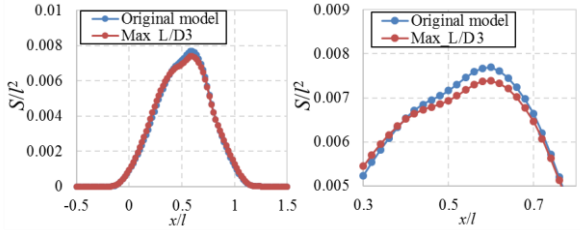

Fig. 11 Equivalent Cross-Sectional Area Distrubtion

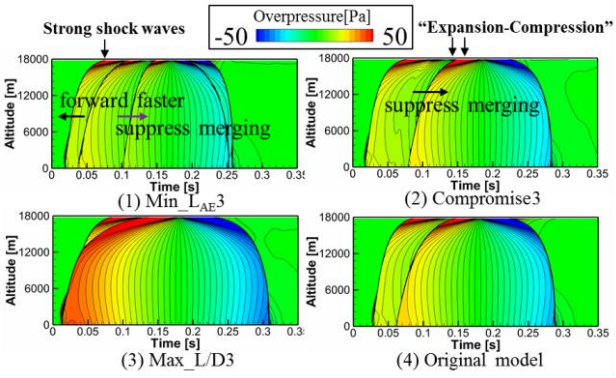

Fig. 12 Visualization of Pressure Propagation

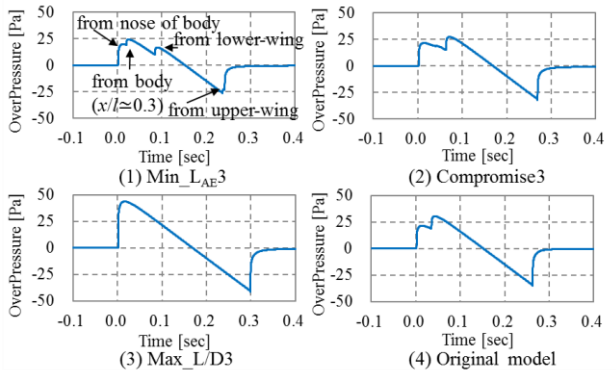

Fig. 13 Sonic Boom Signature at Ground

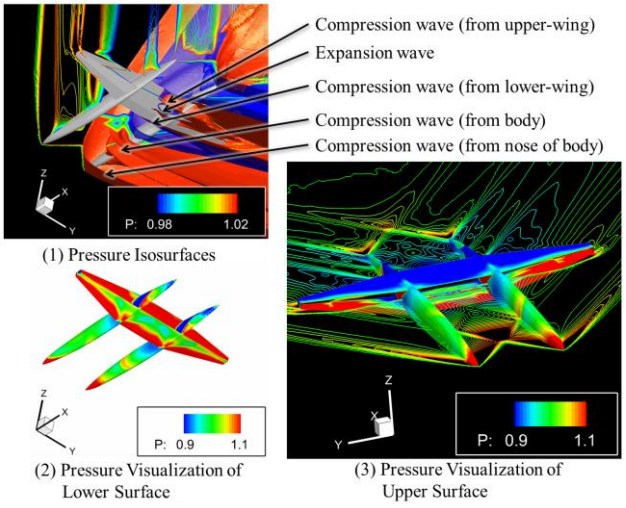

Fig. 14 Pressure Visualizations of Compromised Solution Selected from Pareto Optimal Designs

5 Concluding Remarks

In this research, twin-body fuselage / biplane wing 200 passengers SST models have been discussed. Aerodynamic performance has been evaluated by using inviscid CFD computations. The skin friction drag has also been considered utilizing the standard algebraic (turbulent) skin friction models based on the wetted areas of

SST configurations. Furthermore, sonic boom performance of the innovative SST configurations has also been discussed. Three design optimizations for wing section shape and body shape of the Busemann biplane / twin body configuration have been carried out under the conditions of M_∞ of 1.7 and the angle of attack of 2 degrees. These optimizations are performed to obtain design knowledge for the innovative SST. The maximization of the lift-drag ratio (L/D) and the minimization of maximum overpressure (P_{max}) or A-weighed sound exposure level (L_{AE}) are the objective functions. P_{max} and L_{AE} are the same kind of metrics to evaluate the sonic boom strength.

By the low-boom / low-drag design optimizations, the tradeoff relationship between L/D and P_{max} can be observed. It can be confirmed that the obtained optimal designs have better performance than the original model. It is confirmed that better Pareto optimal solutions are obtained with larger numbers of design variables. Furthermore, we obtained the following design knowledge. (1) The lift-drag ratio is significantly affected by the thickness difference between the upper/lower-wings. (2) The pattern of "expansion-compression" in pressure waveform is important to reduce sonic boom strength. (3) The trailing edge shapes of the wings are important for both lift-drag ratio and sonic boom strength. (4) The nose shape of fuselage is important for the reduction of sonic boom strength. (5) The inner body shape is important for the reduction of interference drag between bodies. (6) It is possible to introduce the supersonic area rule in the twin-body / biplane-wing configuration. In the best cases, one of the obtained optimal designs has achieved 7.32 of lift-drag ratio while another optimal design has achieved 21.7[Pa] of maximum overpressure.

Our final target performance is 8.0 in L/D and 24[Pa] in P_{max} at the present fuselage volume. These target performance values are specified to satisfy twice passenger capacity of Concorde, to have better aerodynamic performance than Concorde, and to have a quarter of P_{max} of Concorde. It is said that the Concorde's performance is 7 in L/D and 2[psf] (96[Pa]) in P_{max}[29]. The optimized model has not yet achieved the target performance, i.e. a compromised model has 6.23 of L/D and 27.3[Pa] of P_{max}. Although the present optimization achieved large improvement in L/D, P_{max} and L_{AE}, the body shape design variables were not yet sufficient to perform detailed shape optimization. Since we have obtained major design knowledge of the innovative SST configuration in this study, the survey of the appropriate definition of the design variables will be performed. Then, the target performances can be realized by reducing more the wing-body interference drag and by controlling the pressure waveform pattern more efficiently. Furthermore, we will also discuss about the structural design, flight stability, off-design performance, and so on for the demonstration of its inclusive availability.

Acknowledgements

I'm very grateful to numerical simulation research group of JAXA for providing me their nonlinear acoustic propagation solver of Xnoise, as well as for their helpful advices.

References

[1] Kusunose, K., Matsushima, K., and Maruyama, D., "Supersonic Biplane—A Review," Progress in Aerospace Sciences, Vol.47, pp.53-87, 2011.

[2] Kusunose, K., Matsushima, K., Obayashi, S., Furukawa, T., Kuratani, N., Goto, Y., Maruyama, D., Yamashita, H., and Yonezawa, M., "Aerodynamic Design of Supersonic Biplane: Cutting Edge and Related Topics," The 21st century COE Program International COE of flow dynamics lecture series, Vol.5, Sendai, Tohoku University Press, 2007.

[3] Matsushima, K., Kusunose, K., Maruyama, D., and Matsuzawa, T., "Numerical Design and Assessment of a Biplane as Future Supersonic Transport," Proceedings of the 25th ICAS Congress, ICAS Paper 2006-3.7.1, Hamburg, 2006.

[4] Matsushima, K., Maruyama, D., Kusunose, K., and Noguchi, R., "Extension of Busemann Biplane Theory to Three Dimensional Wing Fuselage Configurations," Proceedings of the 27th ICAS Congress, ICAS Paper 2010-2.8.1, Nice, 2010.

[5] Yamazaki, W. and Kusunose, K., "Aerodynamic Study of Twin-Body Fuselage Configuration for Supersonic Transport," Transactions of the Japan Society for Aeronautical and Space Sciences, Vol.56, No.4, pp.229-236, 2013.

[6] Sears, W. R., "On Projectiles of Minimum Wave Drag," Quarterly of Applied Mathematics, Vol.4, No.4, pp.361-366, 1947.
[7] Yamazaki, W. and Kusunose, K., "A Biplane Wing / Twin-Body Fuselage Configuration for Innovative Supersonic Transport," Journal of Aircraft, Vol. 51, No. 6, pp. 1942-1952, 2014.
[8] Yamazaki, W. and Kusunose, K., "Innovative Supersonic Transport Configuration by Biplane Wing / Twin-Body Fuselage" Proceedings of the 29th ICAS Congress, ICAS Paper 2014-0735, 2014.
[9] Nakahashi, K., Ito, Y., and Togashi, F., "Some Challenges of Realistic Flow Simulations by Unstructured Grid CFD," International Journal for Numerical Methods in Fluids, Vol.43, No.6-7, pp.769-783, 2003.
[10] Yamazaki, W., Matsushima, K., and Nakahashi, K., "Drag Prediction, Decomposition and Visualization in Unstructured Mesh CFD Solver of TAS-code," International Journal for Numerical Methods in Fluids, Vol.57, No.4, pp.417-436, 2008.
[11] Obayashi, S. and Guruswamy, G. P., "Convergence Acceleration of a Navier-Stokes Solver for Efficient Static Aeroelastic Computations," AIAA Journal, Vol.33, No.6, pp.1134-1141, 1995.
[12] Burg, C. O. E., "Higher Order Variable Extrapolation for Unstructured Finite Volume RANS Flow Solvers," AIAA Paper 2005-4999, 2005.
[13] Venkatakrishnan, V., "On the Accuracy of Limiters and Convergence to Steady State Solutions," AIAA Paper 93-0880, 1993.
[14] Sharov, D. and Nakahashi, K., "Reordering of Hybrid Unstructured Grids for Lower-Upper Symmetric Gauss-Seidel Computations," AIAA Journal, Vol.36, No.3, pp.484-486, 1998.
[15] Ito, Y. and Nakahashi, K., "Surface Triangulation for Polygonal Models Based on CAD Data," International Journal for Numerical Methods in Fluids, Vol.39, Issue.1, pp.75-96, 2002.
[16] Sharov, D. and Nakahashi, K., "Hybrid Prismatic/Tetrahedral Grid Generation for Viscous Flow Applications," AIAA Journal, Vol.36, No.2, pp.157-162, 1998.
[17] Yamamoto, M., Hashimoto, A., Takahashi, T., Kamamura, T., and Sakai, T., "Long-range Sonic Boom Prediction Considering Atmospheric Effects," Proceedings of InterNoise 2011, Osaka, 2011.
[18] Yamamoto, M., Hashimoto, A., Takahashi, T., Kamakura, T., and Sakai, T., "Numerical Simulations for Sonic Boom Propagation through an Inhomogeneous Atmosphere with Winds," AIP Conference Proceedings, Nonlinear Acoustics, pp.339-342, 2012.
[19] Raymer, D. P., "Aircraft Design: A Conceptual Approach Fourth Edition," AIAA Education Series, AIAA, 2006.
[20] Krasnov, N. F., "Aerodynamics of Bodies of Revolution," Edited and Annotated by Morris, D. N., Elsevier, New York, 1970.
[21] "Handbook of Aerospace Engineering: The Third Edition," The Japan Society for Aeronautical and Space Sciences, (eds.), Maruzen, 2005 (in Japanese).
[22] Hu, R., "Supersonic Biplane Design via Adjoint Method," Dissertation for the degree of Doctor of Philosophy, Department of Aeronautics and Astronautics, Stanford University, 2009.
[23] Yamazaki, W. and Mavriplis, D. J., "Derivative-enhanced Variable Fidelity Surrogate Modeling for Aerodynamic Functions," AIAA Journal, Vol.51, No.1, pp.126-137, 2013.
[24] Jones, D. R., Schonlau, M., and Welch, W. J., "Efficient Global Optimization of Expensive Black-Box Functions," Journal of Global Optimization, Vol.13, pp.455-492, 1998.
[25] Fonseca, C. M. and Fleming, P. J., "Genetic Algorithms for Multiobjective Optimization: Formulation, Discussion and Generalization," Proceedings of the 5th International Conference on Genetic Algorithms, Morgan Kaufmann Publishers, Inc., San Mateo, pp.416-423, 1993.
[26] Ban, N. and Yamazaki, W., "Grid Deformation around Junction Regions and its Application to Shape Optimization," Proceedings of 53rd Conference of the Japan Society of Mechanical Engineering, (Hokuriku/Shin-etsu Branch), OS4-1-301, 2016 (in Japanese).
[27] Horinouchi, S., "Conceptual Design of a Low Sonic Boom SSBJ," JAXA Research and Development Report, JAXA-RR-05-045, 2006. (in Japanese).
[28] Makino, Y., Naka, Y., Hahimoto, A., Kanamori, M., Murakami, K., and Aoyama, T., "Sonic Boom Prediction Tool Development at JAXA," Japan Society for Aeronautical and Space Sciences, Vol.61, No.7, pp.237-242, 2013. (in Japanese).
[29] Yoshida, K., "Low Sonic Boom Design Technology for Next Generation Supersonic Transport," Journal of the Acoustical Society of Japan, Vol.67, No.6, pp.245-250, 2011 (in Japanese).

Contact Author Email Address

s101065@stn.nagaokaut.ac.jp

Copyright Statement